Exp Fluids (2010) 48:17–31
DOI 10.1007/s00348-009-0699-1

PAP-1022

RESEARCH ARTICLE

Performance of a combined three-hole conductivity probe for void fraction and velocity measurement in air–water flows

João Eduardo Borges · Nuno H. C. Pereira · Jorge Matos · Kathleen H. Frizell

Received: 24 July 2008 / Revised: 8 June 2009 / Accepted: 10 June 2009 / Published online: 4 July 2009

Abstract The development of a three-hole pressure probe with back-flushing combined with a conductivity probe, used for measuring simultaneously the magnitude and direction of the velocity vector in complex air–water flows, is described in this paper. The air–water flows envisaged in the current work are typically those occurring around the rotors of impulse hydraulic turbines (like the Pelton and Cross-Flow turbines), where the flow direction is not known prior to the data acquisition. The calibration of both the conductivity and three-hole pressure components of the combined probe in a rig built for the purpose, where the probe was placed in a position similar to that adopted for the flow measurements, will be reported. After concluding the calibration procedure, the probe was utilized in the outside region of a Cross-Flow turbine rotor. The experimental results obtained in the present study illustrate the satisfactory performance of the combined probe, and are encouraging toward its use for characterizing the velocity field of other complex air–water flows.

J. E. Borges (✉)
Department of Mechanical Engineering, IDMEC,
Instituto Superior Técnico, Technical University of Lisbon,
Lisbon, Portugal
e-mail: tborges@hidro1.ist.utl.pt

N. H. C. Pereira
Department of Mechanical Engineering, EST Setúbal,
Polytechnic Institute of Setúbal, Setúbal, Portugal
e-mail: npereira@est.ips.pt

J. Matos
Department of Civil Engineering and Architecture,
Instituto Superior Técnico, Technical University of Lisbon,
Lisbon, Portugal
e-mail: jm@civil.ist.utl.pt

K. H. Frizell
U.S. Bureau of Reclamation, Denver, CO 80225, USA
e-mail: khfrizell@usbr.gov

List of symbols

A_{ex}	Nozzle exit area (m^2)
C_{air}	Air concentration or void fraction
C_{pr}	Air concentration indicated by conductivity probe
H	Head applied to turbine (m)
K_i	Coefficient relative to the ith pressure taping
$\dot{m}_{air}$	Air mass flow rate (kg/s)
p_{air}	Air gauge pressure (Pa)
p_{dyn}	Jet dynamic pressure (Pa)
p_i	Pressure at the ith pressure taping (Pa)
p_{mix}	Mixture gauge pressure (Pa)
p_n	Pressure at standard conditions (p_n = 101,325 Pa)
p_s	Static pressure (Pa)
Q_{air}	Air volume flow rate (m^3/s)
Q_n	Air volume flow rate at standard conditions (T_n = 273.15 K and p_n = 101325 Pa) (m^3/s)
Q_{tot}	Total volume flow rate of mixture (m^3/s)
Q_w	Water volume flow rate (m^3/s)
r_{ex}	Nozzle exit radius (m)
R	Ideal gas constant [R = 287 J/(kg K)]
t_{air}	Air temperature (°C)
t_{mix}	Mixture temperature (°C)
T_n	Temperature at standard conditions (T_n = 273.15 K)
U	Rotor tip velocity (m/s)
U/V_0	Blade-jet velocity ratio
V	Local velocity (m/s)
V_j	Velocity of calibrating jet (m/s)
V_0	Jet velocity given as: $V_0 = \sqrt{2gH}$(m/s)
V/V_0	Non-dimensional absolute velocity (m/s)

Greek symbols

α	Absolute velocity angle (degrees)
β	Relative velocity angle (degrees)
γ	Probe rotation angle (degrees)
θ	Rotor peripheral angle (degrees)
ρ_{air}	Air density (kg/m^3)
$\rho_{air,mix}$	Air density in the air–water jet (kg/m^3)
ρ_{mix}	Mixture density (kg/m^3)
ρ_w	Water density (kg/m^3)

Subscripts

air	Relative to the air part of the mixture
dyn	Dynamic
ex	Exit
i	General pressure taping
j	Jet
mix	Relative to the air–water mixture
n	Standard
pr	Probe
s	Static
tot	Total
w	Water

1 Introduction

The study of highly turbulent air–water flows is a complex problem whose solution is often required for the analysis of hydraulic structures, such as spillways and energy dissipators, as well as in some hydraulic turbines like the Pelton and the Cross-Flow. The analytical and numerical approaches are still not a viable option in most cases, leaving as the only alternative the characterization of the desired flow using experimental techniques, namely for the measurement of the air concentration and velocity. A review of some methods traditionally used for performing this task can be found in Jones and Delhaye (1975), Bachalo (1994), Nagash (1994), Ceccio and George (1996), Matos et al. (2002) and Chanson (1997, 2002, 2004). The reviews presented therein demonstrate that this has been an area of significant progress, and among some recent experimental techniques for velocity measurement one can mention the use of particle image velocimetry (PIV), acoustic Doppler velocimetry (ADV), hot-film anemometry, double-tip conductivity probes, double-tip fiber-optical probes and back-flushing Pitot tubes in conjunction with conductivity probes.

In spite of all the progress reported, these methods were found to have their drawbacks. For example, PIV and ADV are limited to applications where the air concentration is less than 5–10% (Amador 2005; Frizell 2000). The use of hot-film anemometry was found to raise difficult questions related with the calibration and interpretation of the measured signals (Cartellier and Achard 1991; Nagash 1994). The double-tip conductivity probes and the double-tip fiber-optical probes may be used for the measurement of the magnitude of the velocity vector, provided that its direction is known beforehand, allowing a previous orientation of the probe with the flow direction (Chanson 1997; Boes and Hager 1998; Matos et al. 2002). Another option that could be employed in similar situations where the velocity direction is known beforehand is the use of back-flushing Pitot tubes in conjunction with conductivity probes. Indeed, the flushing system avoids the presence of air bubbles in the system, whereas the local air concentration provides an estimate of the density of the air–water flow in the vicinity of the stagnation pressure at the upstream end of the tube. This allows the determination of the local velocity. Nevertheless, the velocity data becomes unreliable if the velocity direction departs too much from the assumed direction, or in the case of air concentrations larger than typically 70–80% (Frizell et al. 1994; Chamani and Rajaratnam 1999; Matos et al. 2000).

However, there are situations where the direction of the velocity vector is not known prior to the measurements and varies significantly from point to point in space, such as the flow inside and around the rotor of a Cross-Flow turbine (e.g., Haimerl 1960; Pereira and Borges 1996). Situations analogous to these but with homogeneous flows (one phase) can be treated using one of the experimental techniques reviewed and described in detail in Ower and Pankhurst (1965) and Bryer and Pankhurst (1971). All these methods rely on the use of intrusive pressure probes that take advantage of the pressure distribution that is imparted to the probe surface when it is exposed to a moving fluid. The value of this pressure distribution at discrete locations can be measured using a suitable number of pressure tapings, and the pressure values obtained in this way may provide enough information for the determination of the magnitude and direction of the velocity vectors, provided an appropriate calibration is carried out beforehand. If the flow may be considered two-dimensional, the simultaneous measurement of the magnitude and direction of the velocity vector only requires the pressure values in three tapings or sensing holes, while for measuring three-dimensional flows the probes must have four sensing holes, or preferably, more in order to introduce some redundancy in the technique. The measurement of flow direction can be carried out using two different strategies, namely, the "null-reading" or "fixed-direction" method. In the "null-reading" method, the probe is aligned with the flow so that the pressures in two holes located symmetrically take equal values. When that happens, the probe orientation defines the direction of the velocity vector. For the "fixed-direction" method the probe is not aligned with the flow, resulting in pressure readings that are different in all the

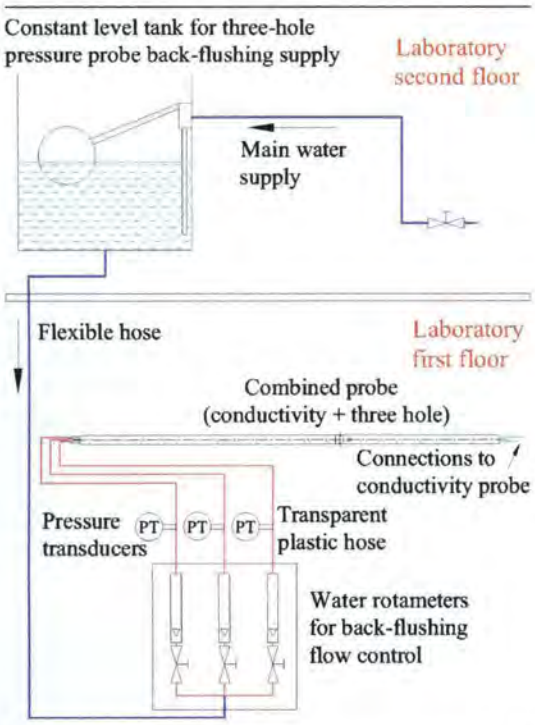

Fig. 2 Sketch of the three-hole pressure probe and back-flushing system

measured using pressure transducers, one for each pressure tube. The pressure transducers are of the gauge type, made by DRUCK, model PTX1400, and have a maximum operating pressure of 1 bar and a typical accuracy of 0.15% of full scale. All the pressure transducers used during the current work were calibrated using a DRUCK pressure calibrator model DPI 610.

For homogeneous flow, the pressures at each of the tapings, p_i, can be related with the static and dynamic pressures using the following equations:

$$p_i = p_s + K_i \cdot p_{dyn}, \quad i = 1, 2, 3 \tag{1}$$

where p_s and p_{dyn} are, respectively, the static and dynamic pressures, K_i are constants to be determined via the calibration process, and where the number 1 will be used for the central hole and the numbers 2 and 3 for the side holes. Due to symmetry considerations, it should be $K_2 = K_3$. In addition, it should be $p_2 = p_3$, whenever the probe is aligned with the flow. Hence, the three equations 1 imply that:

$$p_{dyn} = \frac{p_1 - p_2}{K_1 - K_2} = \frac{p_1 - p_3}{K_1 - K_3} \tag{2}$$

Equation 2 permits the determination of the dynamic pressure, once the three pressures given by the three-hole probe are measured. This value enables the calculation of the velocity magnitude, V, which is given by:

$$V = \sqrt{\frac{2 \cdot p_{dyn}}{\rho}} \tag{3}$$

where ρ is the density of the homogeneous fluid. The alterations due to the fact that the fluid is formed by two distinct phases are dealt with below.

The conductivity probe is formed by two platinum electrodes with a diameter approximately equal to 0.4 mm and separated by a distance of 1 mm (see Fig. 1), mounted in the same cylindrical rod as the three-hole pressure probe and aligned with the central hole (No. 1) of the three-hole pressure probe. The measurement principle of conductivity probes is based upon the large difference in electrical resistivity between water and air. The probe is able to detect air bubbles that contact the electrodes, producing a signal that can be related to the value of the air concentration or void fraction. The electric current, resulting from a voltage whose polarity is reversed periodically (about once every second), is monitored with the electronics control box, which produces an output voltage depending on the air concentration in the air–water mixture where the platinum electrodes of the probe are located (Frizell et al. 1994; Jacobs 1997).

The probe signals were acquired using a National Instruments data acquisition board PCI-6024E with a maximum sampling rate of 200 kHz, inserted inside a personal computer using a Windows XP operating system. Computational programs were developed in LabView programing language, version 6.1, specifically for probe control and output signal acquisition and analysis. The data acquisition was carried out with a sampling rate of 8 kHz during a 60 s interval. Preliminary tests showed that varying the sampling rate between 2 and 12 kHz, and the sampling time period between 20 and 80 s did not significantly influence the measured mean values.

2.2 Calibration rig

The combined probe was calibrated in a specially built calibration rig, using a working principle identical to those described in Bachmeier (1988) or in Frizell et al. (1994). This rig is formed by a constant head water supply that feeds a pipe with 60 mm inside diameter, where compressed air is injected through a porous tube, and is mixed with the water (Fig. 3). The air–water mixture is then forced to pass by several stainless steel meshes to homogenize the flow. At the end of the main pipe, there is a 20 mm diameter exit nozzle, through which the air–water mixture is ejected, forming a free jet that is used for calibrating both components of the combined probe. The combined probe was calibrated in a position similar to that adopted for flow measurements in the turbine rotor, using

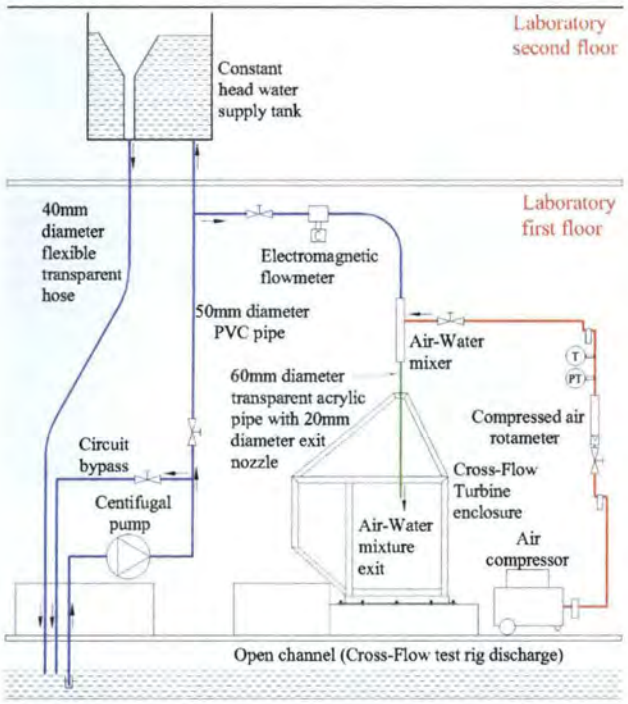

Fig. 3 Sketch of the calibration rig

water coming from the same reservoir that supplies the Cross-Flow turbine rig. Two photographs of the jet issuing from the exit nozzle and used for calibrating the probe can be seen in Fig. 4, where the first photograph is for clear-water flow and the second for an air–water mixture with 40 % air concentration. Figure 5 shows the probe being calibrated using both a clear-water jet and being subjected to an air–water mixture.

The relative position and distance between the nozzle exit and the combined probe could be adjusted to determine if the probe location relative to the nozzle exit was appropriate. The distance was chosen as small as possible but allowing the local static pressure in the jet to reach atmospheric pressure. In order to check whether this condition was fulfilled, it was decided to study the influence of the probe distance on the volumetric flow rate of water leaving the nozzle, instead of directly measuring the static pressure. It was considered that if the probe was placed in a zone where the local static pressure is equal to the atmospheric pressure, it would not have any effect on the volumetric flow rate leaving the nozzle. The influence of the volumetric flow rate on the probe distance from the nozzle was measured and is presented in Fig. 6 for both clear-water and a typical air–water mixture. The results show that the minimum distance for having a negligible change on the volume flow rate is around 20 mm, or a distance equal to about one exit nozzle diameter. Hence, during most of the calibration process the probe was located at a larger distance, namely at 22.5 mm below the nozzle exit, in order to assure atmospheric pressure at that given location.

The air concentration and velocity at the exit of the nozzle are estimated by individually measuring the incoming water and air volumetric flow rates. The water volumetric flow rate, Q_w, is measured prior to the mixing with air using an electromagnetic flow meter ISOMAG, model MS1000-P50-OA1A/ML200-BOA1B2A, with a typical accuracy of 0.2% of the measured value. The air volumetric flow rate is determined using an air rotameter, along with a thermometer and a pressure transducer both positioned at the exit of the rotameter. The rotameter used is a FISHER & PORTER device, model 10A1197, the thermometer is a TESTO unit, model 925, with an estimated maximum error of 0.8°C, and the pressure transducer is a DRUCK apparatus, model PTX1400, with a typical accuracy of ±0.15% of full scale. The readings of the thermometer and pressure transducer allow the determination of the air density, which together with the air volumetric flow rate permits calculation of the air mass

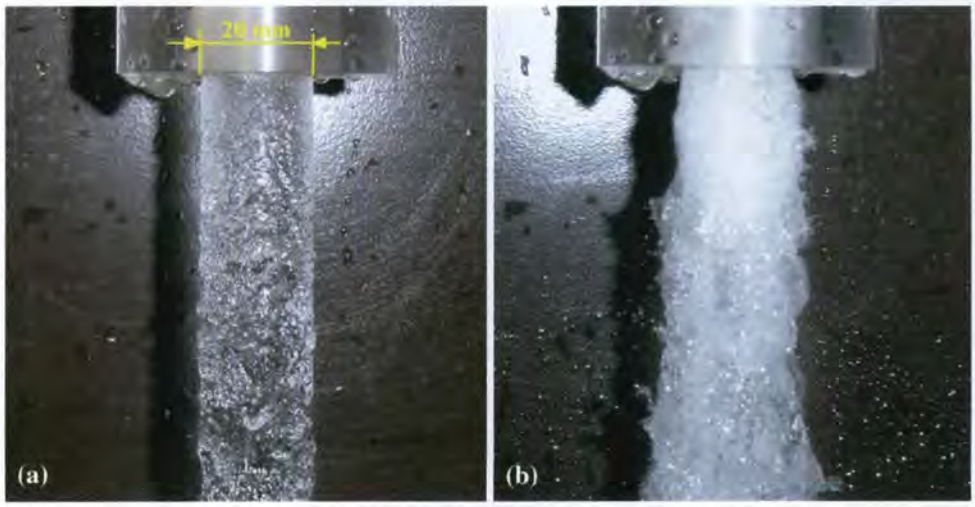

Fig. 4 Calibrating jet: **a** clear-water; **b** air–water mixture

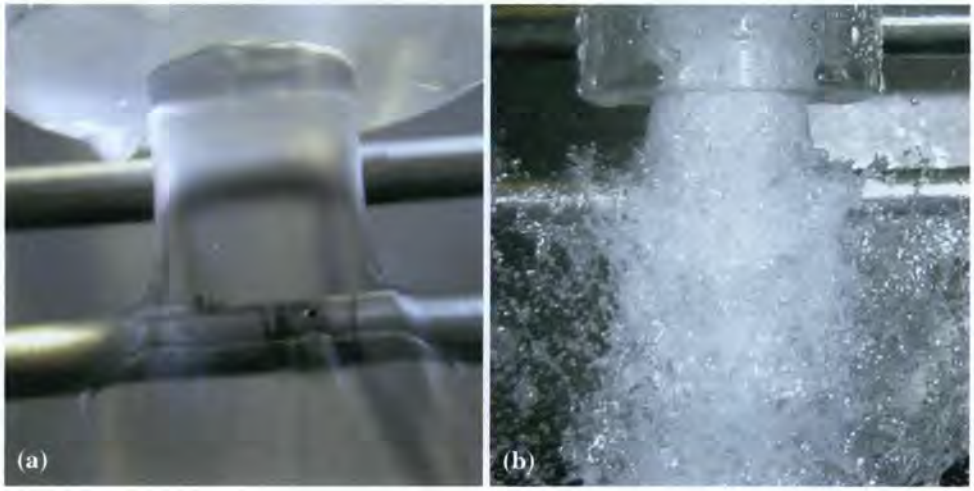

Fig. 5 Combined probe testing: **a** clear-water; **b** air–water mixture

flow rate. In fact, the volumetric flow rate of air passing through the rotameter, Q_{air}, can be calculated by:

$$Q_{air} = \frac{Q_n}{\sqrt{\frac{p_n + p_{air}}{p_n} \cdot \frac{T_n}{T_n + t_{air}}}} \tag{4}$$

where Q_n is the air volumetric flow rate for standard conditions ($T_n = 273.15$ K and $p_n = 101{,}325$ Pa), and p_{air} and t_{air} are, respectively, the measured pressure and temperature of the air at the exit of the rotameter. Once the air volumetric flow rate is known, one can compute the air mass flow rate $\dot{m}_{air}$ using:

$$\dot{m}_{air} = \rho_{air} \cdot Q_{air} = \frac{p_n + p_{air}}{R(T_n + t_{air})} \cdot Q_{air} \tag{5}$$

with ρ_{air} being the air density.

Using the principle of mass conservation, and assuming that the air neither leaves nor enters into the jet issued from the nozzle, it is possible to evaluate the volumetric flow rate in the section of the calibrating jet where the probe is placed as:

$$Q_{air,mix} = \frac{\dot{m}_{air}}{\rho_{air,mix}} = \frac{\dot{m}_{air}}{\frac{p_n + p_{mix}}{R(T_n + t_{mix})}} = \frac{\dot{m}_{air} \cdot 287 \cdot (273.15 + t_{mix})}{101{,}325 + p_{mix}} \tag{6}$$

The air concentration, or void fraction, is defined as being the ratio between the air volume and the total volume of mixture, and can be evaluated by:

$$C_{air} = \frac{Q_{air,mix}}{Q_{tot}} = \frac{Q_{air,mix}}{Q_{air,mix} + Q_w} \tag{7}$$

where Q_{tot} is the total volumetric flow rate of mixture. In the above calculations, it was implicitly assumed that the air concentration distribution is uniform across a section of the calibrating jet. This assumption will be subsequently analyzed and validated.

The calibration process also requires the knowledge of the velocity in the jet. This value will be calculated assuming that the velocity profile is uniform at the nozzle exit, and that the jet maintains the same diameter after leaving the nozzle exit. Therefore, the jet velocity, V_j, is given by:

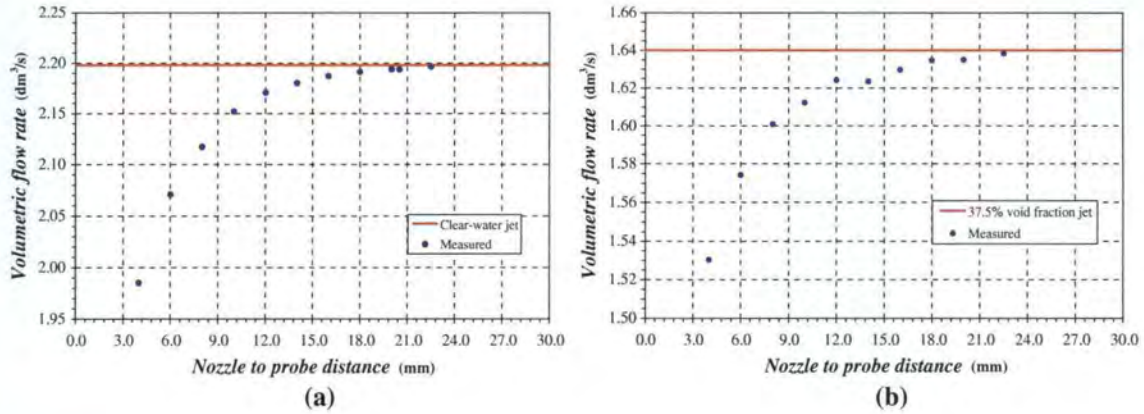

Fig. 6 Influence of the distance between the nozzle and probe on volumetric flow rate: **a** clear-water; **b** air–water mixture

$$V_j = \frac{Q_w + Q_{air,mix}}{A_{ex}} = \frac{Q_w + \frac{\dot{m}_{air} \cdot 287 \cdot (273.15 + t_{mix})}{101{,}325}}{\pi \cdot r_{ex}^2} \quad (8)$$

in case the two phases move with the same velocity (zero slip velocity), and where A_{ex} and r_{ex} are, respectively, the area and radius at the nozzle exit. The dynamic pressure of the jet p_{dyn} is therefore, equal to:

$$p_{dyn} = \frac{1}{2} \cdot \rho_{mix} \cdot V_j^2 \quad (9)$$

with ρ_{mix} being the mixture density given by:

$$\rho_{mix} = \rho_w \cdot (1 - C_{air}) + \rho_{air} \cdot C_{air} \quad (10)$$

and ρ_w is the water density. The term $\rho_{air} \cdot C_{air}$ is usually neglected because it is much smaller than the remaining term. In the above equations, it was implicitly assumed that the flow is homogeneous.

The maximum average velocity that can be achieved with the present calibration rig at nozzle exit, under clear-water flow conditions (zero injection of air) is approximately equal to 9 m/s. Regarding the air concentration, the present calibration rig can produce flows with any desired volumetric air concentration, ranging from clear-water flows, to flows made up entirely of air, i.e., the rig can accommodate a variation of 0–100% in air concentration. However, it was not possible to obtain a homogeneous mixture for air concentrations much larger than about 70%, similar to what has been observed by Frizell et al. (1994) in the Bureau of Reclamation's facility. Further information can be found in Pereira (2007).

2.3 Cross-Flow rig

The combined probe was used to measure the flow at the rotor exit of a Cross-Flow turbine. These measurements were performed in a rig for testing hydraulic turbines, described in detail in Pereira (2007) and Pereira and Borges (1996). The rig is located at the Turbomachinery Laboratory, Instituto Superior Técnico, Technical University of Lisbon. Before entering into the turbine the water is sent to a telescopic tank where the water head is maintained constant by allowing some surplus water to overflow the top of the tank. After passing through the turbine the water is conveyed to a reservoir situated below the laboratory floor. The water is then pumped back from this reservoir to the telescopic tank, closing the hydraulic circuit. The power generated by the turbine is absorbed by a DC motor-generator and can be calculated by measuring the torque applied to the turbine rotor axis and its rotational velocity. The head applied to the turbine is determined using a Pitot tube placed in the inlet duct, where the total pressure is measured with a pressure transducer. The volume flow rate is measured with an electromagnetic flow meter. The knowledge of all these variables permits the calculation of the hydraulic turbine efficiency. A detailed discussion of the instrumentation used to characterize the turbine performance can be found in Pereira (2007). The maximum head that can be attained in this rig is 5.5 m, and the maximum allowable volume flow rate is about 0.1 m^3/s. A sketch of the Cross-Flow turbine is presented in Fig. 7. Also shown therein is the path used for the flow traverses

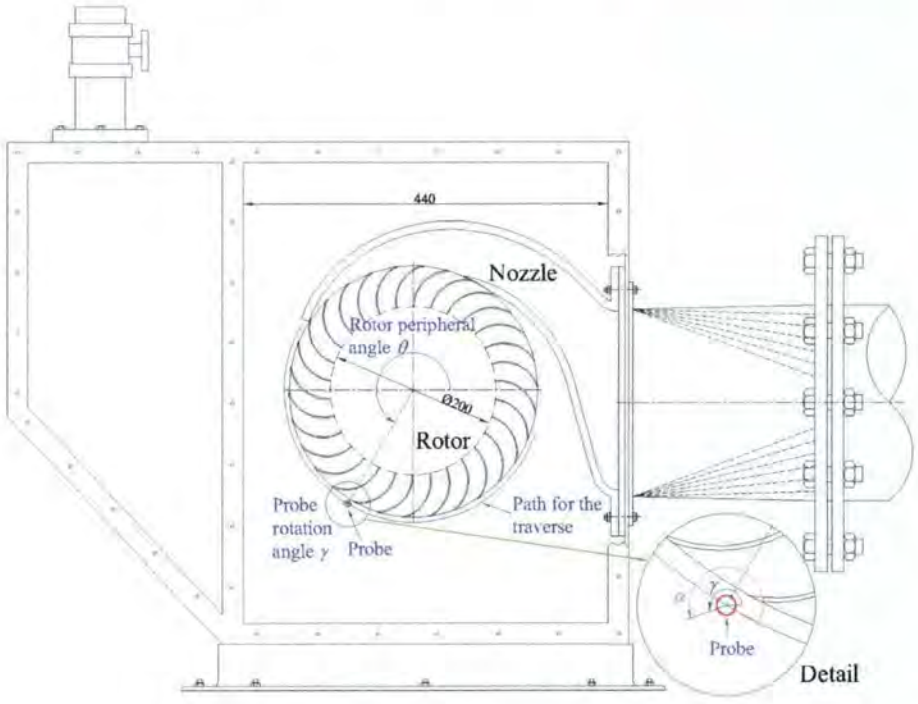

Fig. 7 Sketch of the Cross-Flow turbine test rig, with the path used for traverses of the combined probe indicated

with the combined probe and the rotor, which has an outside diameter of 300 mm. The width of the rotor (dimension perpendicular to the plane of Fig. 7) is 210 mm and the rotor has 30 blades. Other dimensions of the turbine can be inferred from Fig. 7 and its inset, since both were drawn approximately at scale. Further characteristics of the Cross-flow turbine can be found in Pereira (2007).

The mechanism that supports the combined probe allows the movement of the probe along paths of constant radius, at the outside of the rotor. This mechanism was also used during the calibration process. The probe orientation in space and location along the traverse path are determined by the measurement of two angles, as illustrated in Fig. 7. The probe orientation gives directly the velocity vector direction, whenever the probe is aligned with the flow. These two angles were measured using two angular displacement sensors able to read 0.1 of a degree.

3 Probe calibration

3.1 Conductivity component

The conductivity component of the combined probe was calibrated by subjecting it to an air–water jet of varying air concentrations generated by the calibration rig. During preliminary tests it was found essential to have the water and all the metal components of the apparatus in contact with it suitably grounded, to get an appropriate response from the conductivity probe. This was done by connecting the ground of the electronics control box with the water, the probe supporting mechanism, and to the ground of the main electrical supply. Before conducting any tests, the conductivity probe and respective electronics control box was switched on and left exposed to the flow for a period of around 30 min to avoid any thermal transients that could affect the probe output voltage. Another verification done systematically prior to the tests consisted in balancing the conductivity probe in a clear-water jet. With this procedure it was guaranteed that the voltage applied to the electrodes was exactly symmetrically reversed during each cycle (see Jacobs 1997). After concluding this verification, the detection voltage threshold was adjusted. Typically, a voltage threshold of between 0.02 and 0.06 V was used in the present tests.

Prior to probe calibration two series of tests were performed to assess the probe behavior under severely varying conditions. The first set of tests studied the probe response to the flow orientation relative to the probe electrodes. This verification was important to determine the sensitivity of the measured results for air concentration in case the probe was not properly aligned with the flow as conceivably could happen during measurements in the turbine. During these tests the probe was rotated relative to the jet, and the values of air concentration directly indicated by the electronics control box without any correction resulting from calibration, as a function of the probe rotation angle are presented in Fig. 8. This figure also gives the values of the jet air concentration using measured air and water values and computing the air concentration from Eq. 7. An analysis of the plot reveals that the air concentration indicated by the electronics control box stayed almost constant for probe rotations of almost 20° on both sides of zero rotation, suggesting that the probe has a very low sensitivity to rotation. This turned out to be a positive feature of the probe, and facilitates its use. It should also be noted that when the probe rotation is increased toward large values, the amount of air detected by the probe is increased. This may be due to the large values of pressure associated with the stagnation line along the probe that deflect the smallest air bubbles away from the electrodes when aligned with the flow, leading to a measurement of air concentration that is smaller than in reality. When the probe is rotated, the electrodes move away from the stagnation line, enabling the detection of the smallest air bubbles deflected from the stagnation line, and increasing the measured air concentration.

The second tests performed prior to probe calibration studied the air concentration uniformity across the jet diameter, to assess the quality of the assumptions that lead to Eq. 7. These tests were done using the probe to perform traverses of the jet, and taking note of the value of air concentration given directly by the electronics control box. Two different types of traverses were carried out, one along the probe axis, called longitudinal traverse, and the other perpendicular to the probe axis, called lateral traverse. The results, presented in Fig. 9a, b indicate that the jet has a core radius of about 6 mm, where the air concentration distribution directly indicated by the electronics control box is practically uniform. In these figures, the level of air

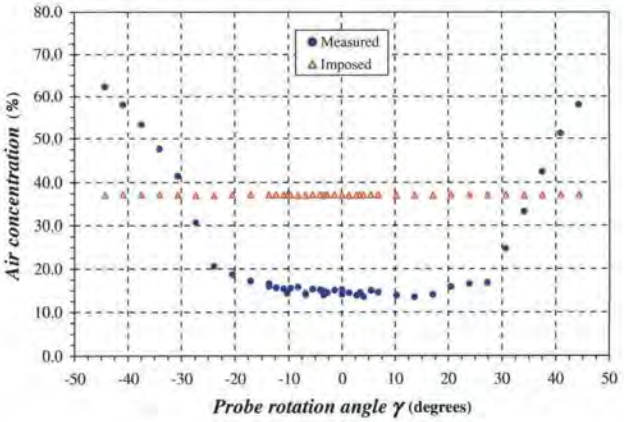

Fig. 8 Influence of the probe rotation on indicated air concentration

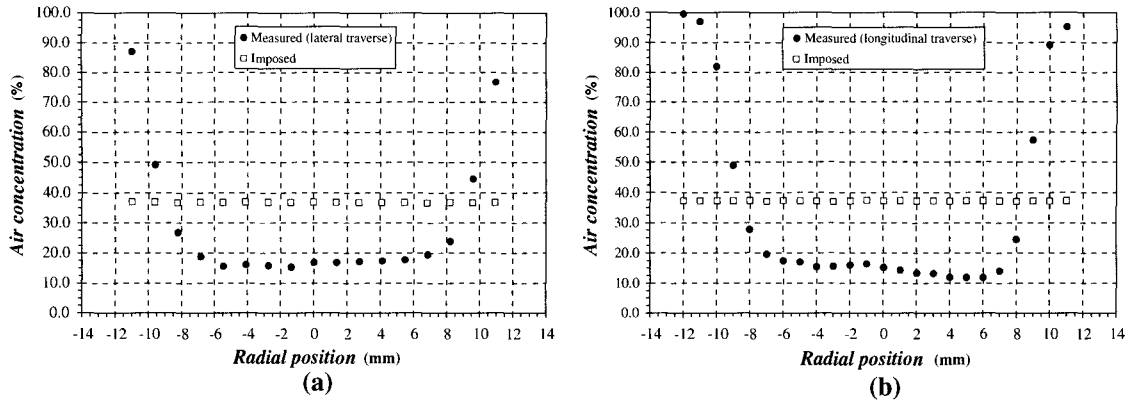

Fig. 9 Traverses of the air–water jet used to determine the region of the jet where probe performance is adequate: **a** lateral traverse; **b** longitudinal traverse

concentration calculated using Eq. 7 is also shown. The fact that the jet presents a core where the air concentration is practically uniform validates the calibrating procedure adopted in the present study, based on the use of a free jet, and also found in other studies (see Matos and Frizell 2000). In fact, if the gradient of air concentration is zero in the jet core, one can conclude that in the jet core there was no air diffusion normal to the flow direction. Hence, it is also safe to conclude that the air concentration in the core maintained an identical value as that at the exit plane of the calibrator nozzle, and was not influenced at all by any eventual air entrained at the free jet boundary after leaving the nozzle. A similar reasoning can be applied to the velocity magnitude, with the corresponding alterations. It should also be noticed that these traverses seem to imply that the jet radius is slightly greater (around 11–12 mm) than the radius of the exit orifice of the nozzle (10 mm), suggesting that there may exist some air entrainment from the surroundings and some jet deflection due to the probe.

After concluding these preliminary tests, the calibration of the conductivity probe was performed by comparing the air concentration produced by the calibration rig and calculated from Eq. 7, with the output of the electronics control box that was connected to the conductivity probe, maintaining the probe aligned with the flow. All the experimental data acquired during the calibration tests are plotted in Fig. 10, along with the regression curves used to fit the experimental data. The scatter evident in Fig. 10 can be justified by the existence of additional factors that have a second order influence on the probe behavior, and in order to give an idea of the possible interference of these factors on the measurements to be performed, large variations in their magnitude were considered during the calibration process. So, during the acquisition of the calibrating points, the velocity magnitude varied from 2.5 to 15 m/s, the voltage threshold from 0.02 and 0.06 V, and the distance between the probe and the nozzle exit from 10 to 26 mm. In addition, two different nozzle geometries for the exit nozzle of the calibrating rig were employed, both with and without back-flushing on. Figure 10 indicates that the overall probe response is non-linear, presenting a region where the probe reading is zero or nearly zero, although there is already some air mixed with water in the jet. This failure of the probe to detect air bubbles persists until values of the jet air concentration of around 15%. The reduced accuracy of the probe in detecting low air concentrations may be due to the probe geometry, which causes a flow stagnation in the electrodes region, and eventually to the size of the probe tips. The pressure increase in the vicinity of the measuring location is expected to move small air bubbles away from the tips of the electrodes. In the range between 25 and 75%, the probe has an almost linear output. For air concentrations above 70% the calibration rig is unable to provide a homogeneous flow, even though the probe signal was considered consistent. It should also be noted that the experimental data exhibit some scatter, varying from –6.0 to 3.7% for values of the indicated air concentration at the electronics control box greater than 1%. However, the greatest difference was detected when an air concentration of 16.5% was imposed in the jet, and the probe failed to detect any air concentration, indicating a zero value.

The measured probe response was approximated using two curves, which are also presented in Fig. 10, and are defined by the equations:

$$C_{air}(\%) = \begin{cases} 0 & C_{pr} = 0\% \\ 10.158 - 10.204 \cdot C_{pr} + 2.507 \cdot C_{pr}^{1.5} - & \\ 0.204 \cdot C_{pr}^{2} + 20.79 \cdot C_{pr}^{0.5} & 0\% < C_{pr} \leq 7.3\% \\ 8.232 \times 10^{-10} \cdot C_{pr}^{6} - 1.897 \times 10^{-7} \cdot C_{pr}^{5} + & \\ 1.478 \times 10^{-5} \cdot C_{pr}^{4} - 3.771 \times 10^{-4} \cdot C_{pr}^{3} - & C_{pr} > 7.3\% \\ 6.262 \times 10^{-3} \cdot C_{pr}^{2} + 1.128 \cdot C_{pr} + 22.631 & \end{cases} \quad (11)$$

These equations were used in the measurements for calculating the true air concentration starting from the value indicated by the electronics control box connected to the conductivity probe.

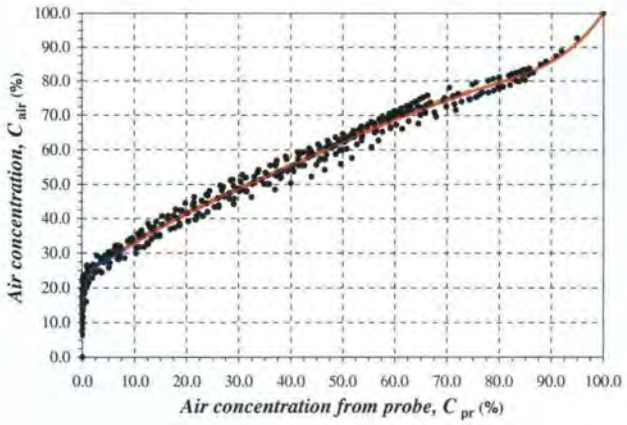

Fig. 10 Calibration curve of the conductivity component

3.2 Three-hole component

The three-hole pressure component of the combined probe was calibrated by placing it in the jet issuing from the calibration rig and subjecting it to different values of flow direction and magnitude, as illustrated in Fig. 5. The velocity at nozzle exit was calculated assuming a uniform velocity profile at the exit, and the individual values of the pressure at the probe pressure tapings were measured for each flow condition.

Similar to the conductivity component, some preliminary tests were conducted prior to the probe calibration to evaluate the probe behavior under severely varying conditions. The first series of tests studied the influence of the amount of back-flushing on the probe response, to check whether the three pressure lines exhibited similar pressure drop. These tests were performed by subjecting the combined probe to both clear-water and air–water jets. The results are presented in Fig. 11a, b, which reveal that all the individual pressure measurements follow approximately similar quadratic evolutions with respect to the amount of back-flushing. The plots also demonstrate that the pressure lines experience almost the same reaction with the variation of back-flushing, both with and without air mixed in the water jet, for values of back-flushing approximately smaller than 0.4 dm^3/h. It should be noted that in the jet being studied the value of the stagnation pressure is equal to the dynamic pressure because the gauge static pressure has a zero value (the jet static pressure is equal to the atmospheric pressure). A correction for the difference in pressure attributable to the back-flushing was introduced in all subsequent measurements in accordance with the present results. The next set of tests studied the variation of pressures in the three tapings, as a function of the dynamic pressure of the jet when using a clear-water jet. The results obtained in these experiments are given in Fig. 12, which show a linear variation of all the pressures with the dynamic pressure imposed by the jet. Using the measured values for the pressures on the sensing holes it is possible to calculate the constants K_i for the three tapings, resulting respectively,

$$K_1 = 1.01; \quad K_2 = -0.21; \quad K_3 = -0.22 \tag{12}$$

These values for the constants are analogous to those presented in Lewis (1965), for the classic cylindrical three-hole pressure probe, used to measure in homogeneous air flows.

The following tests evaluated the influence of probe rotation on the pressure measurements. The output of these tests are shown in Fig. 13a for a clear-water jet, and in Fig. 13b for an air–water mixture of 26% air concentration and a back-flushing rate equal to 0.26 dm^3/h. The curves of Fig. 13a are almost symmetrical relative to the angle of 0°, as is expected due to symmetry considerations, and they show a sudden increase in the pressure at the side holes for probe angle orientations of around 4–5°. Such sudden increase can be justified by the passage of the flow separation line (line visible in Fig. 5a) by the side holes. This fact increases the probe sensitivity to a misalignment with the flow direction. It should also be noted that for the

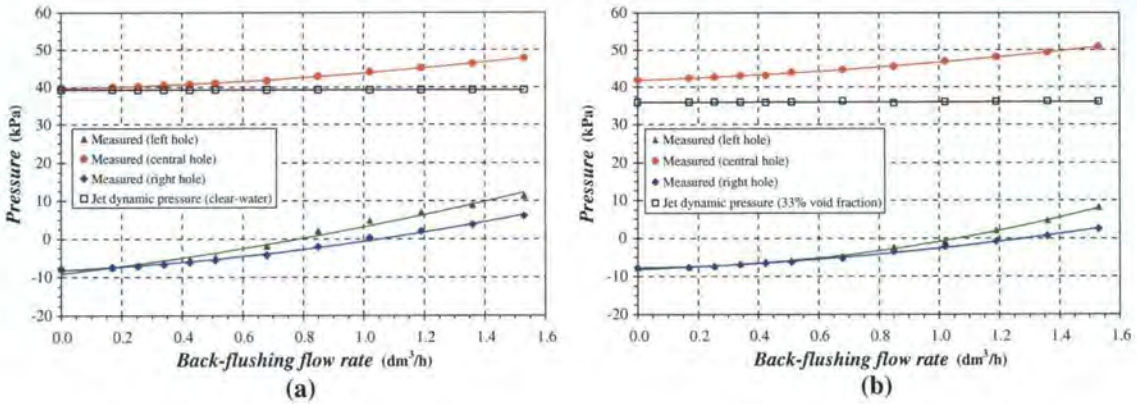

Fig. 11 Influence of back-flushing flow rate on measured pressure probe response: **a** clear-water; **b** air-water mixture

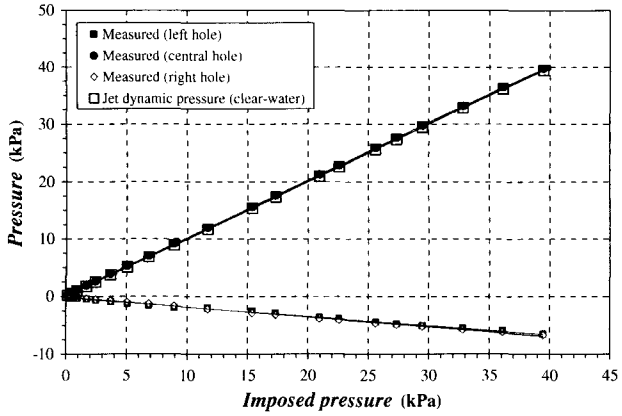

Fig. 12 Influence of imposed dynamic pressure on measured probe response (back-flushing rate: 0.26 dm^3/h)

amount of probe rotation considered, the pressure registered by the central hole is practically constant and equal to the stagnation pressure of the jet. For an air–water mixture the results obtained are presented in Fig. 13b, where the sudden pressure increase due to passage of the flow separation line is not so clearly marked, although still be detected. The measurement of the velocity vector was done with the probe aligned with the flow, implying that the probe rotation angle will be around 0°. Figure 13a, b illustrates that for such condition both side holes measure identical pressure values.

A verification of the velocity uniformity at the nozzle exit was then studied to assess the validity of the assumptions used to derive Eq. 8. This verification was done by performing longitudinal traverses of the jet, measuring the local velocity at several points. The outcome of the longitudinal traverses is presented in Fig. 14a, using no back-flushing and in Fig. 14b for a back-flushing flow rate of 0.54 dm^3/h, which is a value slightly greater than the back-flushing flow rate typically used in the remaining experiments (0.26 dm^3/h). Comparing both figures, it is evident that the back-flushing rate does not introduce any relevant modification in the results, because the values on both plots are almost coincident. In addition, it is seen that the jet has a core with a radius of approximately 7 mm, where the velocity is quite uniform, and has values very close to those imposed, which are calculated using Eq. 8. This validates the approximations proposed earlier. As the probe approaches the jet boundary, it starts to measure velocity magnitude values that decay smoothly and tend

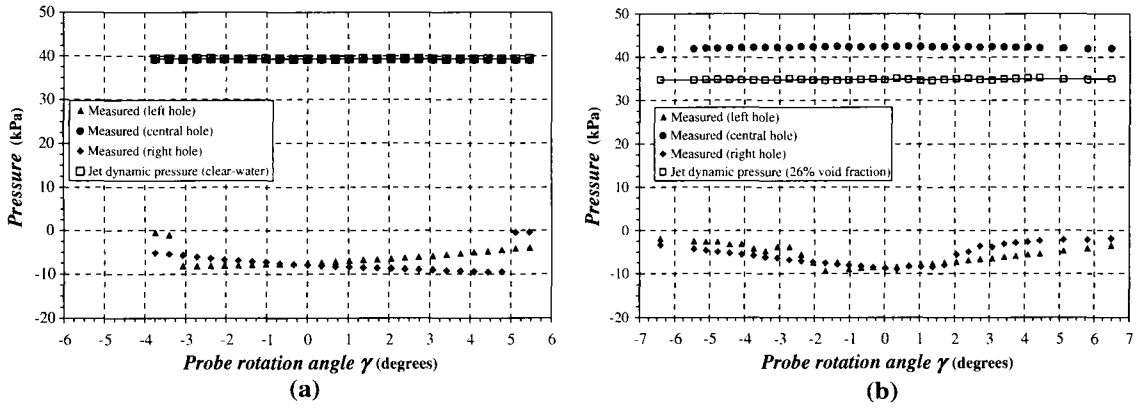

Fig. 13 Influence of probe rotation on measured probe response (back-flushing rate: 0.26 dm^3/h): **a** clear-water; **b** air-water mixture

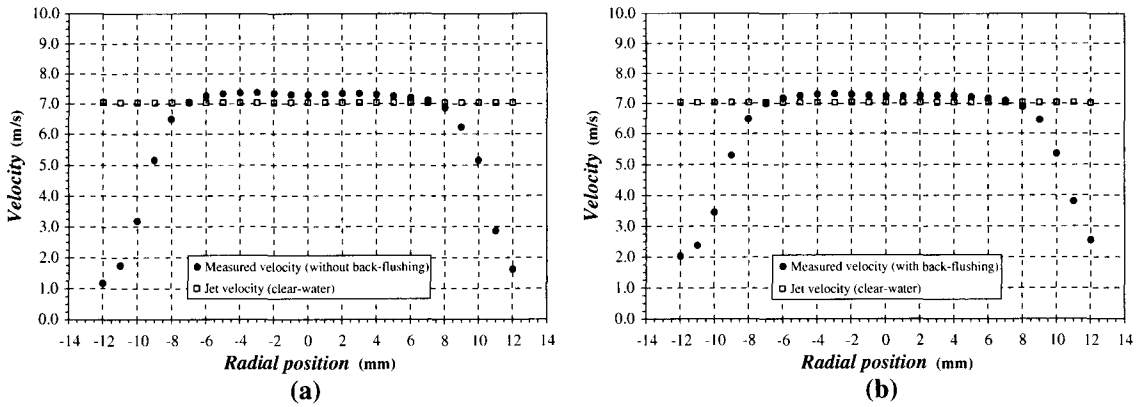

Fig. 14 Longitudinal traverse of the clear-water jet used for probe calibration: **a** without back-flushing; **b** with back-flushing (0.54 dm^3/h)

toward zero for a radius greater than the nozzle exit radius. In fact, this must be so partly due to jet deflection caused by the probe, and partly due to the fact that the jet radius increases slightly after leaving the nozzle.

A lateral traverse of the jet where the probe was moved perpendicularly to its axis was also done using a clear-water jet. The results of these lateral traverses are displayed in Fig. 15a, which applies to a traverse where the probe was moved with the orientation fixed in space, and in Fig. 15b, which applies to a traverse where the probe was aligned with the local velocity direction. In this last case, the local velocity direction is also indicated in the plot. These lateral traverses, besides confirming the previous conclusion that the jet has a nucleus with uniform velocity, also gave some indications of the possible experimental errors incurred when using the present pressure probe near jet boundaries (regions where there is a large variation in void fraction), due to the interaction of the probe with the jet. In fact, Fig. 15a shows that the misalignment of the probe increases and leads even to flow separation, when the probe approaches the jet boundary. Figure 15b shows that the error in the velocity orientation may amount to 5° when the probe is situated at a distance of one probe diameter from the jet boundary, and for closer boundary distances, one may have even larger errors, on the order of 10°. However, it should be stressed, that this conclusion is affected by the way in which the probe approaches the jet boundary, because the longitudinal traverses do not show these effects. It should also be noted that the error in the determination of the velocity direction seems not to contaminate the value of the velocity magnitude, since both Fig. 15a, b evidence a good agreement between the measured velocity magnitude and the value calculated using Eq. 8, for most of the points considered in the traverses, including even points located less than one probe diameter from the jet boundary.

After the orientation and uniformity checks, the influence of the air concentration of the air–water mixture at the nozzle exit was studied. During this calibration the air concentration was varied, and the pressure difference measured between the central hole and the average pressure at the side holes was divided by the dynamic pressure estimated at the nozzle exit. The results are plotted in Fig. 16, where it can be seen that the experimental points closely follow a curve, which was fitted using the following fifth degree polynomial as a function of the air concentration of the air–water mixture:

$$p_{dyn} = p_1 \cdot \left(\begin{array}{l} 4.098 \times 10^{-9} \cdot C_{air}^5 - 6.663 \times 10^{-7} \cdot C_{air}^4 + 3.523 \times 10^{-5} \cdot C_{air}^3 - \\ 3.808 \times 10^{-4} \cdot C_{air}^2 - 1.154 \times 10^{-2} \cdot C_{air} + 1.019 \end{array} \right)$$
$$0\% < C_{air} \leq 70\% \qquad (13)$$

where p_1 is the gauge pressure measured in the central hole and p_{dyn} is the dynamic pressure. In this equation, advantage was taken of the fact that, for the present measurements, the static pressure will be always equal to the atmospheric pressure. Further information about the calibration process and other tests can be found in Pereira (2007).

4 Results

The combined probe performance was assessed in a real measurement environment by traversing the probe and

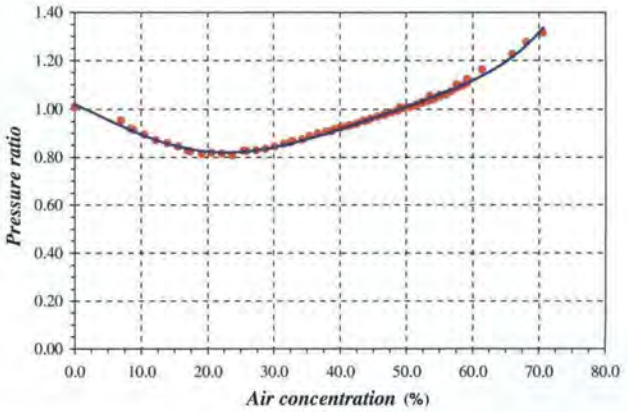

Fig. 16 Calibration curve of the three-hole pressure component (back-flushing rate: 0.26 dm^3/h)

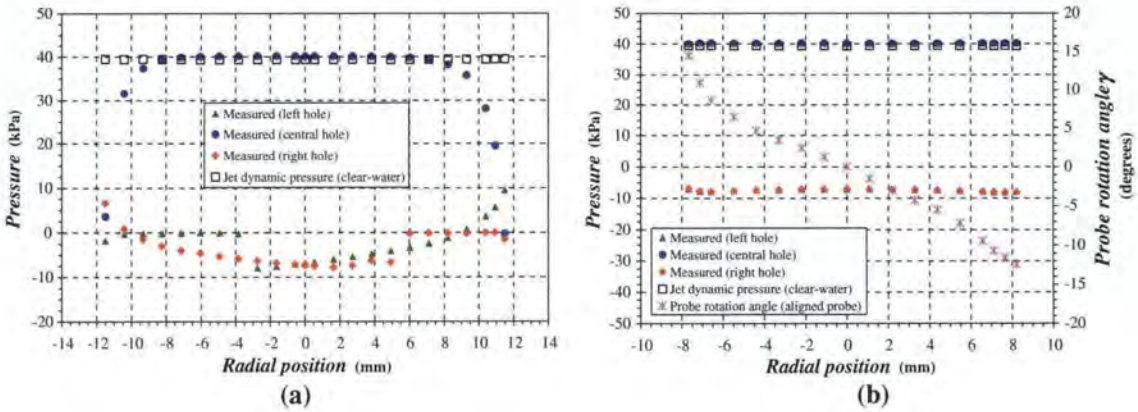

Fig. 15 Lateral traverse of the clear-water jet used for probe calibration: **a** maintaining the probe fixed; **b** aligning the probe with the flow field

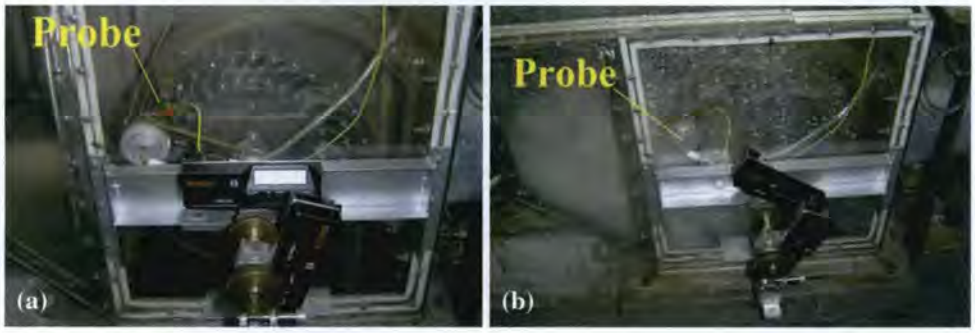

Fig. 17 Combined probe located outside of the Cross-Flow turbine rotor: **a** without flow; **b** with flow

collecting both the magnitude and direction of the velocity vectors at the exit of the rotor of a Cross-Flow turbine, as shown in Fig. 7. In this figure, the path taken during the traverses and the two angles θ and γ used to determine the location and orientation of the probe are also included. Figure 17a, b are photographs of the Cross-Flow rig, without and with flow, respectively, showing the supporting mechanism used for performing the traverses and for measuring the two angles θ and γ. Both angles θ and γ were measured with origin at the first quadrant horizontal axis, as indicated in Fig. 7. The angle γ directly provides the probe orientation, while the angle θ permits the calculation of the probe location given that the traverses were carried out for a constant radius, with the probe axis located at a radius of 157.5 mm, and in the clockwise direction (which is contrary to the rotor rotation). The data presented in the following plots were measured for peak-efficiency conditions of the Cross-Flow turbine, an operating condition that occurred for a value of the blade to jet velocity ratio $U/V_0 = 0.46$, where U is the rotational velocity of the rotor outside diameter, and V_0 is the jet velocity. The head used in the tests was maintained approximately equal to 3 m.

The traverses were performed with the combined probe by first aligning the probe with the flow at each point, resulting in values of p_2 equal to p_3, and then measuring the air concentration, C_{pr}, the pressure at the central hole, p_1, the probe rotation angle, γ, and the rotor peripheral angle, θ. The probe rotation angle, γ, can be related with the absolute velocity angle, α, measured counter-clockwise from the tangential direction, using simple reasoning (see details of Fig. 7). Values of the absolute velocity angle, α, equal to $-90°$ mean that the flow is radially outwards. The measured value of air concentration, C_{pr}, allows the calculation of the true air concentration, C_{air}, using Eq. 11 obtained from the calibration of the conductivity component. Afterward, using the measured value of p_1, and the calculated value of air concentration, C_{air}, it is possible to compute the local dynamic pressure using Eq. 13 obtained from the calibration of the three-hole pressure component. Finally, the velocity magnitude is obtained from Eq. 3, where the density of the air–water mixture is estimated from Eq. 10. All the values of velocity magnitude were then normalized by the jet velocity V_0 for plotting, i.e., it is the non-dimensional value V/V_0 that is displayed in Fig. 20.

The values of air concentration, C_{air}, versus peripheral angle, θ, at rotor exit and for peak-efficiency conditions are plotted in Fig. 18. The plot shows a wide range of values, spanning from 0% (clear-water) to almost 100% (air only). However, for peripheral angles varying between 220 and 270°, the air concentration, C_{air}, is zero indicating a region where the jet leaving the rotor has small amounts of air and carries most of the water from the inside of the rotor. The failure of the probe in detecting air in the above interval of peripheral angles should be interpreted as a probe limitation, because it is unable to detect low air concentrations, as discussed in Sect. 3.1. This fact could also explain the sudden variation of the air concentration curve near the boundaries of the above interval.

Figures 19 and 20 display the calculated absolute velocity angle, α, and the measured absolute velocity magnitude, respectively, as a function of the peripheral angle, θ. These figures reveal that in the region occupied by the water jet leaving the rotor (interval of peripheral angles between 220 and 270°) both the direction and magnitude show a smooth evolution, with the magnitude of the absolute velocity remaining almost constant and equal to

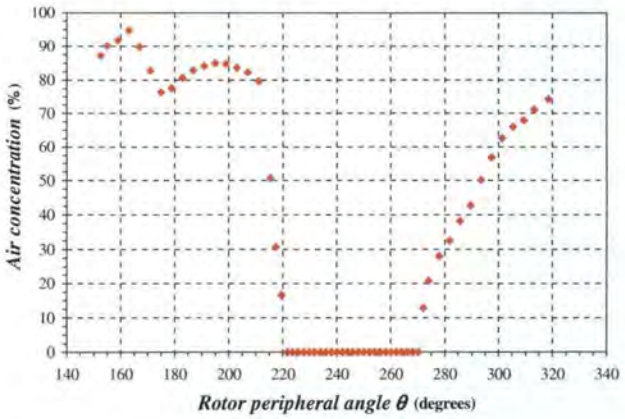

Fig. 18 Measured air concentration of the flow leaving the rotor ($U/V_0 = 0.46$)

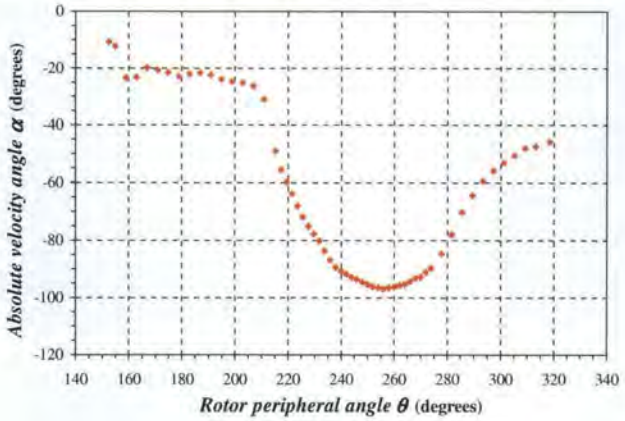

Fig. 19 Measured absolute velocity angle of the flow leaving the rotor ($U/V_0 = 0.46$)

$V/V_0 \cong 0.28$. Outside this interval there are larger variations in the direction and magnitude values, and the evolutions are much less smooth, particularly the absolute velocity angle which varies from -100 to $-20°$, corresponding to flows moving opposite to the rotor direction to flows moving in the same direction of the rotor. It should also be recognized that in a significant portion of the above referenced interval of peripheral angles, the flow direction approaches $-90°$, meaning that most of the water leaves the rotor radially for peak efficiency conditions, which seems a plausible conclusion.

As previously discussed, the tests reported in Fig. 15b seem to suggest that the combined probe may furnish erroneous readings near jet boundaries that are less than one probe diameter from zones where the air concentration varies rapidly. In the present case, one probe diameter corresponds to a variation of peripheral angle approximately equal to 2°, and there are large variations of air concentration for peripheral angles, θ, near 220 and 270°. Figures 19 and 20 show no deleterious effects due to this probe behavior, aside from some data scatter that are evident in Fig. 20 for the velocity magnitude, near the jet limits. Inside the interval corresponding to the leaving jet, where most of the water passed and where it is most important to have accurate measurements, the results seem reasonable.

Using the measured values of direction and magnitude of the absolute velocity, it is possible to obtain the velocity triangle at rotor exit, by vectorially subtracting the transport velocity at the blade exit. This procedure permits the calculation of the relative velocity angle, β, at rotor blade exit, where this angle is considered positive for a counter-clockwise rotation, starting from the tangential direction pointing toward the rotor rotation. The estimated values of the relative velocity angle, β, calculated for the jet leaving the rotor (interval of peripheral angles between 220° and 270°) are plotted in Fig. 21 versus peripheral angle, θ and compared with the level indicated with the word "nominal" that refers to the blade exit angle, which is $-165°$ (value calculated from the relation $-180° + \beta' = -180° + 15°$, see Haimerl 1960). The data presented in the plot follow a smooth variation, the difference between the measured and nominal values being approximately constant. This fact suggests that the flow deviation at blade exit is approximately constant ($\sim 15°$). This last conclusion would be almost impossible to obtain, without the contribution from the combined probe whose development is described in the present paper, and was never put forward before, for this type of turbine.

5 Conclusions

By assembling in a single cylindrical rod a three-hole pressure probe and a conductivity probe, it was possible to develop a new probe capable of simultaneously measuring the velocity magnitude and direction of complex air–water

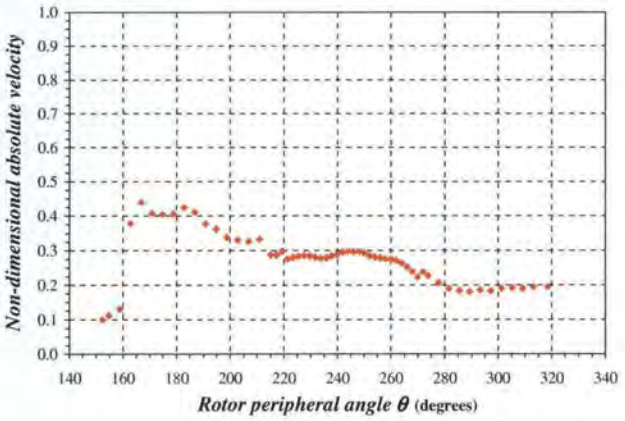

Fig. 20 Measured non-dimensional absolute velocity of the flow leaving the rotor ($U/V_0 = 0.46$)

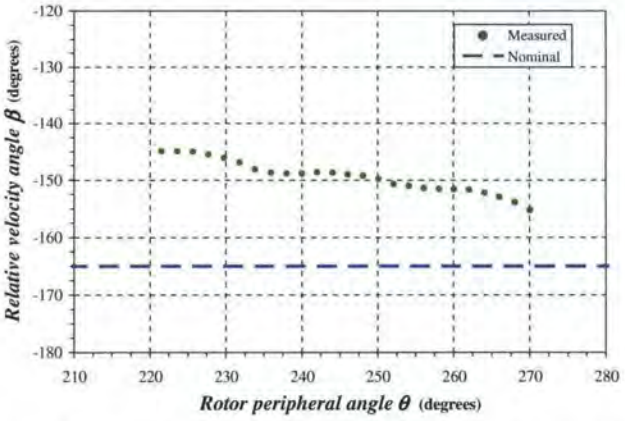

Fig. 21 Calculated relative velocity angle of the flow leaving the rotor ($U/V_0 = 0.46$)

flows, such as those typically found at the exit of Cross-Flow turbine rotors.

A calibration rig was built and used to test and calibrate the combined pressure and conductivity probe. Some preliminary tests were conducted in this calibration rig in order to understand the probe behavior and gain confidence in its output. The calibration curves for both components (conductivity and three-hole pressure) were obtained by subjecting the combined probe to air–water jets of varying velocity and air concentration.

The combined probe was placed outside of a Cross-Flow turbine rotor and several measurements were performed in order to assess the adequacy of this new probe design. The measurements consisted of constant radius traverses of the flow field leaving the turbine rotor. The data obtained in the experiments confirm that the probe performance is suitable for complex air–water flows with unknown flow direction, and it even allowed some important insight into the Cross-Flow turbine performance. In fact, the traverse data seem to suggest that at the rotor exit the blade flow deviation is approximately constant, a conclusion that was never put forward before, for this type of turbine.

6 Further research

Further research should be conducted both concerning the combined probe behavior and the analysis of the Cross-Flow turbine. Concerning the Cross-Flow turbine, further traverses both at the exit and in the inside region should be carried out. In addition, other operating conditions, different from peak-efficiency conditions should be considered. Concerning the combined probe, it would be interesting to develop a new design with a more linear response, in order to improve the accuracy of the measurements for low air concentrations.

Acknowledgments The authors gratefully acknowledge the financial support granted by Fundação para a Ciência e Tecnologia (project PTDC/ECM/73867/2006), as well as the assistance given by the Hydraulic Investigations and Laboratory Services Group of the U.S. Bureau of Reclamation, the IDMEC, the IST-UTL and the EST Setúbal-IPS.

References

Amador A (2005) Comportamiento hidráulico de los aliaderos escalonados em presas de hormigón compactado. PhD dissertation, Universitat Politècnica de Catalunya (UPC), Barcelona (in Spanish)

Bachalo WD (1994) Experimental methods in multiphase flows. Int J Multiph Flow 20(Suppl):261–295

Bachmeier G (1988) Setup, calibration and use of a measuring probe for determination of air concentration in a spillway chute. Diploma dissertation, Institute for Hydromechanics of Karlsruhe University, Karlsruhe, Germany (translated from the German original by Duncan Anderson, USBR)

Boes RM, Hager WH (1998) Fiber-optical experimentation in two-phase cascade flow. In: Proceedings of international RCC dams seminar, Denver, EUA

Bryer DW, Pankhurst RC (1971) Pressure-probe methods for determining wind speed and flow direction. National Physical Laboratory, Her Majesty's Stationery Office, Department of Trade and Industry, London, UK

Cartellier A, Achard JL (1991) Local phase detection probes in fluid/fluid two-phase flows. Rev Sci Instrum 62(2):279–303

Ceccio SL, George DL (1996) A review of electrical impedance techniques for the measurement of multiphase flows. Trans ASME J Fluids Eng 118:391–399

Chamani MR, Rajaratnam N (1999) Characteristics of skimming flow over stepped spillways. J Hyd Eng ASCE 105(4):361–368

Chanson H (1997) Air bubble entrainment in free-surface turbulent shear flows. Academic Press, London

Chanson H (2002) Air-water flow measurement with intrusive, phase-detection probes: can we improve their interpretation? J Hyd Eng 1–4

Chanson H (2004) Air-water flows in water engineering and hydraulic structures. basic processes and metrology. In: Proceedings of international conference on hydraulics of dams and river structures, pp 3–16

Frizell KW (2000) Effects of aeration on the performance of an ADV. In: Proceedings of 2000 joint conference on water resources engineering and water resources planning and management, ASCE, Minneapolis, USA (CD-ROM)

Frizell KH, Ehler DG, Mefford BW (1994) Developing air concentration and velocity probes for measuring in highly-aerated, high-velocity flow. In: Proceedings of hydraulic engineering conference, ASCE, Buffalo, pp 268–277

Fukutomi J, Senoo Y, Nakase Y (1991) A numerical method of flow through a Cross Flow runner. JSME Int J Ser II 34(1):44–51

Haimerl LA (1960) The Cross-Flow turbine. Water Power 12(1):5–13

Jacobs ML (1997) Air concentration meter electronics package manual. Project Notes 8450-98-01, U.S. Department of Interior, Bureau of Reclamation, Denver, USA

Jones OC, Delhaye J-M (1975) Transient and statistical measurement techniques for two-phase flows: a critical review. Int J Multiph Flow 3:89–116

Lewis WE (1965) Fixed-direction probes for aerodynamic measurements. Proc Inst Mech Eng 180(Pt 3J):141–152

Matos J, Frizell KH (2000) Air concentration and velocity measurements on self-aerated flow down stepped chutes. In: Proceedings of 2000 joint conference on water resources engineering and water resources planning and management, ASCE, Minneapolis, USA (CD-ROM)

Matos J, Frizell KH, André S, Frizell KW (2002) On the performance of velocity measurement techniques in air-water flows. In: Proceedings of hydraulic measurements and experimental methods 2002 conference, EWRI-ASCE/IAHR, Estes Park, Colorado, USA (CD-ROM)

Nagash BW (1994) Void fraction measurement techniques for gas-liquid bubbly flows in closed conduits: a literature review. In: Proceedings of hydraulic engineering conference, ASCE, Buffalo, pp 278–288

Ower E, Pankhurst RC (1965) Measurement of air flow, 4th edn. Pergamon Press, New York

Pereira NHC (2007) Estudo de uma Turbina 'Cross-Flow'. PhD dissertation, Technical University of Lisbon, Lisbon (in Portuguese)

Pereira NHC, Borges JE (1996) Study of the nozzle flow in a cross-flow turbine. Int J Mech Sci 38(3):283–302